Fluorescent Nanobodies for enhanced guidance in digestive tumors and liver metastasis surgery

Mateusiak, L.; Hakuno, S.; Jonge-Muller, E.S.M. de; Floru, S.; Sier, C.F.M.; Hawinkels, L.J.A.C.; Hernot, S.

European Journal of Surgical Oncology 51 (2025) 109537

Contents lists available at ScienceDirect

European Journal of Surgical Oncology

journal homepage: www.ejso.com

Fluorescent Nanobodies for enhanced guidance in digestive tumors and liver metastasis surgery

Łukasz Mateusiak [a,*], Sarah Hakuno [b,1], Eveline S.M. de Jonge-Muller [b,1], Sam Floru [a], Cornelis F.M. Sier [c], Lukas J.A.C. Hawinkels [b], Sophie Hernot [a]

[a] Vrije Universiteit Brussel (VUB), Molecular Imaging and Therapy Research Group, MITH, Laarbeeklaan 103, 1090, Brussels, Belgium
[b] Leiden University Medical Center (LUMC), Department of Gastroenterology and Hepatology, Albinusdreef 2, 2333 ZA, Leiden, the Netherlands
[c] Script-Aid, 2132 EG, Hoofddorp, the Netherlands

ARTICLE INFO

Keywords:
Nanobodies
Urokinase plasminogen activator receptor
Fluorescence-guided surgery
Fluorescence molecular imaging
Liver metastasis

ABSTRACT

Background: Fluorescence molecular imaging, a potent and non-invasive technique, has become indispensable in medicine for visualizing molecular processes. In surgical oncology, it aids treatment by allowing visualization of tumor cells during fluorescence-guided surgery (FGS). Targeting the urokinase plasminogen activator receptor (uPAR), overexpressed during tissue remodeling and inflammation, holds promise for advancing FGS by specifically highlighting tumors.

This study explores the extended use of Nanobody-based (Nb) anti-uPAR tracers, evaluating their receptor binding, ability to visualize and demarcate colorectal (CRC) and gastric cancer (GC), and detect localized (PC) and metastatic (PC-M) pancreatic carcinoma.

Methods: First, the receptor structure interactions of Nb15, which binds specifically to the human homologue of uPAR, were characterized *in vitro* to deepen our understanding of these interactions. Subsequently, Nbs 15 and 13—where Nb13 targets the murine uPAR homologue—were labeled with the s775z fluorescent dye and validated in a randomized study in mice (n = 4 per group) using orthotopic human CRC, GC, and PC models, as well as a mouse PC-M model.

Results: Nb15, which binds to the D1 domain of uPAR and competes with urokinase's binding fragment, showed rapid and specific tumor accumulation. It exhibited higher tumor-to-background ratios in CRC (3.35 ± 0.75) and PC (3.41 ± 0.46), and effectively differentiated tumors in GC (mean fluorescence intensity: 0.084 ± 0.017), as compared to control Nbs. Nb13 successfully identified primary tumors and liver metastases in PC-M models.

Conclusion: The tested fluorescently-labeled anti-uPAR Nbs show significant preclinical and clinical potential for improving surgical precision and patient outcomes, with Nb15 demonstrating promise for real-time surgical guidance.

1. Introduction

Despite recent therapeutic advancements, surgical resection remains the first pilar of cancer therapy, aiming for complete tumor removal while minimizing harm to surrounding tissues. With technological progress, oncologic surgery is increasingly enhanced by various modalities, including real-time molecular-targeted fluorescence guidance. This technique employs fluorescent probes that selectively bind to tumor-specific molecules, improving precision by clearly delineating the boundaries between healthy and diseased tissue, highlighting occult lesions, and reducing the invasiveness of surgeries [1].

Since late 2021, there has been a significant clinical advancement in fluorescence agents used for surgical procedures. The first FDA-approved targeted agent for fluorescence-guided surgery (FGS) was Cytalux™ (pafolacianine) [2], targeting the folate receptor for surgical resections of ovarian [3] and lung [4,5] cancer. In April 2024, Lumisight™ (pegulicianine), the first FDA-approved activatable probe, became available. Lumisight™ becomes activated in a cathepsin-rich environment which is characteristic for the tumors [6], aiding in the intraoperative detection of cancerous tissue after lumpectomy surgery

* Corresponding author.
E-mail address: Lukasz.Mateusiak@vub.be (Ł. Mateusiak).
[1] These authors contributed equally to this work.

https://doi.org/10.1016/j.ejso.2024.109537
Received 19 September 2024; Received in revised form 4 November 2024; Accepted 5 December 2024
Available online 6 December 2024

[7]. Numerous other fluorescent tracers are currently undergoing clinical trials, offering promising prospects for further advancements and approvals in the field [8].

To assure broad tracer application potential in FGS, the optimal scenario entails targeting molecules that are expressed by a wide range of different cancers. In this context, one of the receptors that has garnered substantial attention is the urokinase plasminogen activator receptor (uPAR). This is because of its tendency to exhibit overexpression in response to pathological changes in the organism, including inflammation and tissue remodeling, while maintaining low levels in physiological conditions. uPAR's expression has been reported in various human cancers, encompassing solid tumors, leukemias and lymphomas [9–11]. Furthermore, next to cancer cells, uPAR is also expressed on tumor stromal cells [9,12–14], contributing to highlighting the entire tumor rather than the malignant cells exclusively. Consequently, uPAR targeting offers considerable potential in the context of FGS, particularly for the precise delineation of solid tumor margins where tissue remodeling is most pronounced.

Recently, we have reported on the development, comprehensive *in vitro* characterization, and application of Nanobody®(Nb)-based anti-uPAR tracers in an orthotopic glioma model [15]. There, we selected two lead high affinity compounds, Nbs 15 and 13, which bind respectively to human (HuPAR) or murine (MuPAR) receptor homologues. Following fluorescent labeling with the highly photostable near-infrared (NIR) dye s775z, these compounds exhibited rapid tumor targeting, resulting in high tumor-to-background ratios (TBRs). We opted for Nbs rather than peptides or full-size antibodies due to their excellent specificity, rapid targeting, and fast renal clearance, offering advantages over long-circulating tracers by swiftly achieving relevant TBRs [16].

In this study, we further explored the potential of Nbs 15 and 13. We assessed Nb15's binding patterns to the receptor and confirmed its rapid, specific accumulation in cell-line- and patient-derived xenograft (CDX and PDX, respectively) models for human colorectal cancer (CRC), gastric cancer (GC) and localized pancreatic cancer (PC). Additionally, we investigated MuPAR-targeting Nb13 for detecting metastases in a pancreatic cancer metastasis model, considering the contribution of uPAR stromal expression. The results support the tracer's applicability for rapid visualization of various cancers and tracking metastatic spread, paving the way for future clinical translation.

2. Materials and methods

2.1. Nb production and s775z-labeling

Nbs specific to HuPAR or MuPAR, denoted as Nb15 and Nb13, respectively, along with the non-targeting control Nb R3B23 [17], were produced and labeled with the s775z fluorophore via NHS ester-activated crosslinking on lysines [18] according to established methods as described previously [15].

2.2. Flow cytometry

HEK cell lines were scraped at confluency and 1.5×10^5 cells per condition were resuspended in PBS and transferred to Falcon® tubes (Corning Inc.). Cells were stained in cold FACS buffer (PBS, 0.5 % BSA) with 1 μg/mL primary anti-HuPAR antibody (ATN-617) for 30 min, followed by secondary antibody-AF488 (A-21202 Invitrogen) staining as a positive control. To test Nb binding, cells were incubated with 100 nM Nb15 or control Nb R3B23, followed by anti-His-PE staining (clone GG11-8F3.5.1, Miltenyi Biotec). All steps were performed in the dark. Cells were analyzed using a BD LSRFortessa™ flow cytometer and FlowJo software (BD Biosciences).

2.3. Surface plasmon resonance (SPR)

To assess possible competition between anti-HuPAR Nb15 and the natural ligand urokinase (uPA) on the HuPAR receptor, SPR experiments were conducted on a Biacore T200 system (Cytiva). The recombinant HuPAR was immobilized on CM5 sensor chip (Biacore Series S Sensor Chip CM5; Cytiva) as detailed in prior work [15]. Subsequently, the amino-terminal fragment of uPA (ATF) responsible for uPAR binding and the tested Nb were diluted 1:1 in HEPES buffered saline (HBS; Cytiva) to achieve a final concentration 40 times greater than their dissociation constant (K_D). ATF and Nb15 were sequentially introduced onto the sensor chip and then in reverse order to assess potential competition.

2.4. Orthotopic cancer models

In the CRC model, a CDX tumor (HT-29, 2×10^6 cells) was grown subcutaneously in a donor mouse, harvested at 500 mm^3, cut into 3–5 mm^3 pieces, and transplanted into the cecum. For the GC model, a PDX tumor was cut into 8–10 mm^3 pieces and sutured into the gastric wall. In the PC model, 3.5×10^5 BxPC3 cells were injected into the pancreas, and for the PC-M model, 2×10^4 KPC3 cells were injected into the spleen as previously described [19].

2.5. In vivo tumor-targeting, ex vivo quantification and histological analysis

Four weeks after gastric PDX or two weeks after CRC, PC, and PC-M tumor implantation, mice were injected intravenously with 2 nmol of Nb13-s775z (PC-M) or Nb15-s775z (other models), with a non-targeting control (R3B23-s775z) as comparison. Fluorescence imaging (FLI) was performed 1 h post-injection. KPC3-tumor mice were imaged using IVIS Spectrum; CRC, GC, and PC mice were imaged with Pearl Impulse and BLI. *Ex vivo* TBRs were calculated using regions of interest for tumor and adjacent healthy tissue.

Excised tumors and healthy tissues were paraffin-embedded, sectioned, and examined by fluorescence microscopy. Immunohistochemistry (IHC) was performed with anti-uPAR antibodies, followed by staining with biotinylated secondary antibodies and DAB (see Supporting **information**). Slides were then dehydrated, mounted, and imaged using an optical microscope.

2.6. Statistical analyses

Statistical analysis of fluorescently-labeled Nbs' uptake was conducted using Prism v.10.0.3. The number of mice allocated to each experiment was determined based on an a priori power analysis using G*power v.3.1. To assess Nb uptake in tumors and specific organs, alongside the corresponding analysis of mean fluorescence intensities (MFIs) and TBR, a one-tailed Mann-Whitney test was employed, comparing the results to the control R3B23-s775z. The results are described as mean ± SD. Each animal experiment included 4 mice per group, with a total of 32 mice allocated for the study. Statistical significance was set at $p < 0.05$ (*$p < 0.05$, **$p < 0.01$).

3. Results

3.1. Receptor binding characterization

Binding of high-affinity Nb15 (K_D = 2.1 nM) [15] to HEK cells expressing the full human uPAR (D1D2D3) was confirmed (Fig. 1A). This binding was not observed in HEK cells expressing the cleaved receptor (D2D3) or in cells transfected with the empty vector (EV), which do not express the receptor. Importantly, the positive control (ATN-617), specific to the D2D3 domains [20,21], bound both versions but showed dramatically reduced binding to the cleaved receptor. The results suggest that the presence of domain D1 is crucial for efficient uPAR binding by both compounds.

The receptor saturation study confirmed that Nb15 has a higher

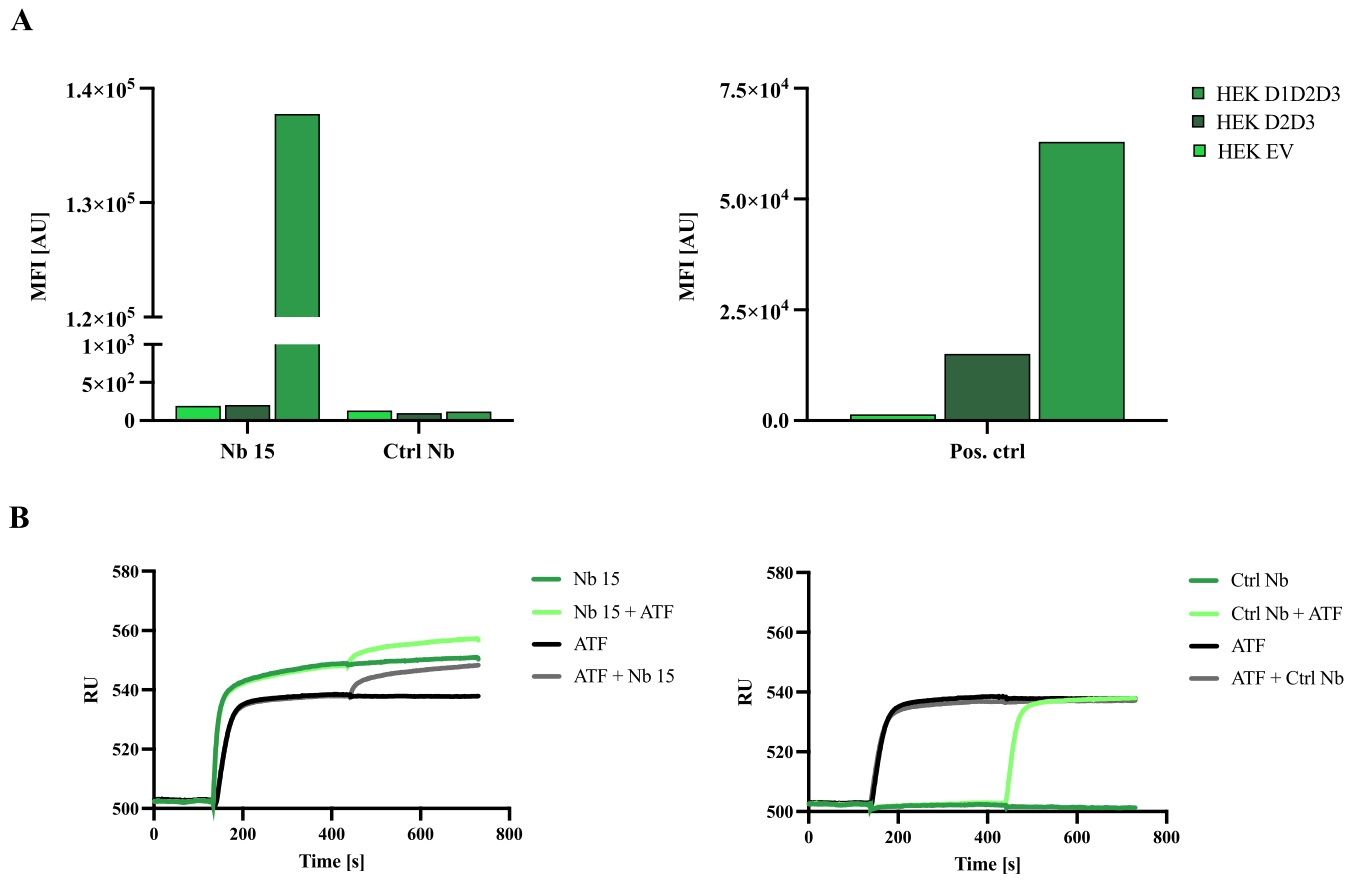

Fig. 1. **(A)** Flow cytometry was conducted on Nb15 and control Nb labeled with PE, targeting two transfected HEK cell types: one expressing full uPAR (D1D2D3) and the other expressing its cleaved variant (D2D3). The obtained mean fluorescence MFI values were compared to those of a negative control cell line (EV) (left) and a positive control targeting D2D3 specifically (ATN-617), labeled with AF488 (right). **(B)** Sensograms of Nb15 (left) and non-targeting control Nb (right), illustrating the competitive interaction for the HuPAR receptor between the targeting Nb and ATF. ATF – amino-terminal fragment of urokinase, Nb - Nanobody.

association rate constant compared to ATF (16.*10^5 vs 6.2*10^5 $M^{-1}s^{-1}$ [15,22]) and a higher receptor affinity than the ATF (difference of 45 RU vs 35 RU during the analyte association, Fig. 1B). The addition of Nb15 or ATF to a pre-saturated receptor resulted in an additional ~10 RU change in resonance, indicating at least partial competition between Nb15 and ATF, as shown in the representative sensogram (Fig. 1B). The control Nb did not cause any change in RU. Nb13 was excluded from these studies due to its affinity for the murine homologue of the

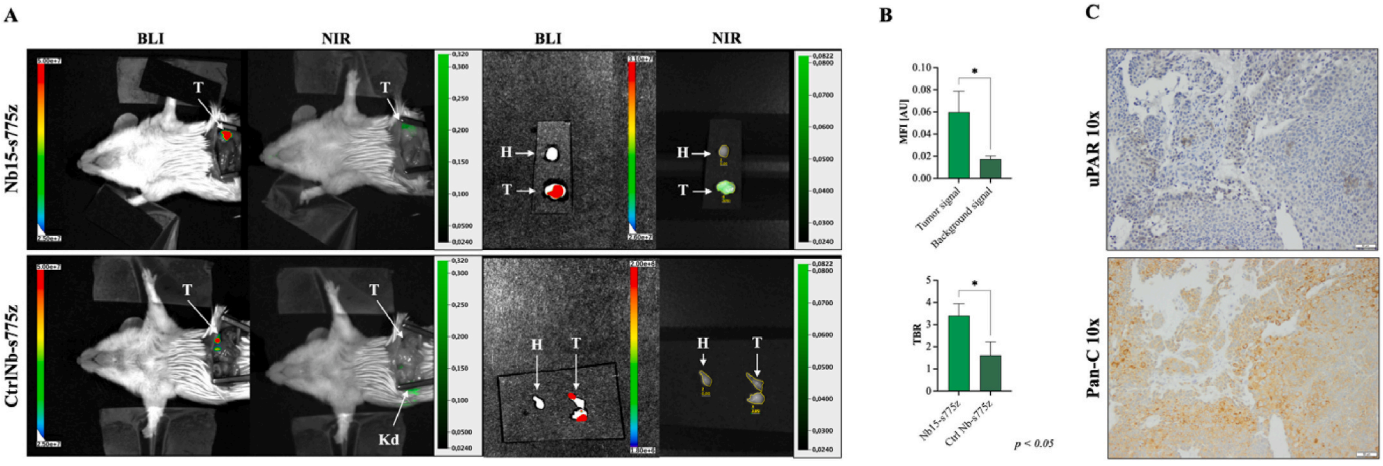

Fig. 2. **(A)** *In situ* (left) and *ex vivo* (right) BLI for monitoring cancer progression and NIR imaging for assessing the distribution of targeting Nb15-s775z and non-targeting control Nb-s775z in mice with CDX orthotopic pancreatic tumors. *T* indicates tumor, *Kd* indicates kidney, and *H* indicates healthy tissue. **(B)** Evaluation of the *ex vivo* signal intensity for the targeting Nb, and comparison of TBRs obtained for the tested tracers. Error bars depict SD. **(C)** Microscopic visualization of IHC staining on consecutive tumor slices shows brown staining of tumor cells expressing uPAR (targeted receptor) overlapping with malignant epithelial cells stained ochre against pan-cytokeratin (Pan-C). (For interpretation of the references to color in this figure legend, the reader is referred to the Web version of this article.)

receptor.

3.2. *In vivo targeting of localized and metastatic tumors using fluorescently-labeled Nbs: quantification and histological analysis*

All three Nbs were successfully labeled with the NIR fluorescent dye s775z using amine-reactive conjugation chemistry **(Supplementary Fig. 1).**

The effectiveness of targeting orthotopic PC with anti-HuPAR Nb15-s775z was confirmed by NIR fluorescence colocalizing with BLI (Fig. 2A). *Ex vivo* imaging showed specific tumor tracer uptake with minimal background, while the non-targeting Nb showed no significant tumor uptake. Fluorescence in kidneys was due to renal clearance, typical for Nb-based tracers. Tumor MFIs were significantly higher for the targeting tracer compared to healthy pancreas (0.060 ± 0.019 vs. 0.017 ± 0.003, $p < 0.05$, Fig. 2B), and the TBR was higher for the targeting tracer than for the non-targeting Nb (3.41 ± 0.46 vs. 1.61 ± 0.49, $p < 0.05$, Fig. 2B). Tumor uPAR positivity was confirmed by IHC (Fig. 2C).

In the subsequent *in vivo* experiment with Nb15-s775z, tumor targeting was compared across CRC and GC models using orthotopic tumors from donor mice or patients. Fluorescence imaging showed clear tumor targeting in both models, with no specific signal from the non-targeting control Nb. Non-specific signals from the kidneys and bladder did not interfere with tumor detection (Figs. 3A and 4A). *Ex vivo* imaging post-resection revealed clear tumor delineation. TBRs were significantly higher for the targeting tracer than the control in the CRC model (3.35 ± 0.75 vs. 1.88 ± 0.60, $p < 0.01$, Fig. 3B). In the GC model, a significantly higher tumor fluorescence was measured for targeting tracer than the control (0.084 ± 0.017 vs. 0.035 ± 0.011, $p < 0.05$, Fig. 4B). Tumor uPAR positivity was confirmed by IHC (Figs. 3C and 4C).

In the final *in vivo* experiment, anti-murine uPAR Nb13-s775z was used to track metastases in a CDX allograft model. BLI confirmed tumor implantation in the spleen and metastasis to the liver, with NIR fluorescence colocalizing with BLI (Fig. 5A). Imaging showed substantial tracer uptake in splenic tumors and hepatic metastases, unlike the control Nb. The targeting tracer had a significantly higher TBR (3.11 ± 1.36 vs. 1.13 ± 0.15, $p < 0.05$) (Fig. 5B). Histology confirmed specific fluorescence in metastatic lesions and uPAR positivity (Fig. 5C).

4. Discussion

The primary goal of this study was to validate the suitability of fluorescently-labeled Nb15-s775z, previously tested in a glioma model, for targeting PC, CRC, and GC tumors, and assess the potential of anti-uPAR Nbs for tracking PC metastases to the liver. Anti-MuPAR Nb13-s775z was used in a PC-M model to visualize metastases by targeting uPAR expressed in the entire tumor, not just cancer cells. We also analyzed anti-HuPAR Nb15's interaction with the receptor to gain deeper insights into its *in vivo* behavior. Preclinical testing of Nb15 and Nb13 in CRC, GC, PC, and PC-M models showed rapid tumor targeting and delineation within 1 h, extending anti-uPAR Nbs' applicability beyond glioma.

As previously discussed, there is a significant contribution of the stromal component of the tumor to uPAR expression [9,12–14]. Due to lead Nb15's lack of cross-reactivity with MuPAR, the specific tumor signal observed is likely lower since the stromal cell contribution to the total signal is not considered. We circumvented this limitation in the murine model by using a high-affinity anti-MuPAR tracer, to compensate for this loss of signal. We used this Nb in the model for metastasis tracking as metastatic lesions can be very small and therefore subtracting the stromal component inclusion poses risk of omitting them whatsoever. In the PC-M cells, Nb13-s775z allowed highlighting of the distant hepatic lesions with significantly higher TBR (3.11 ± 1.36) for the targeting tracer as compared to the control Nb (1.13 ± 0.15) (Fig. 5B). This gives promise for the further translation of our anti-HuPAR compound. These data could have been strengthened by employing IHC staining of different types of uPAR-expressing tumor components (e.g., malignant epithelial and stromal cells), as has been previously demonstrated in human rectal cancer. This technique takes advantage of different epitopes becoming available depending on cell-specific protein interactions [23]. However, identifying antibodies that stain different uPAR types in a mouse model is both costly and challenging, and the tumor growth pattern may not accurately mimic spontaneous cancer in humans. Additionally, the results would be only semi-quantitative, and the distribution of different uPAR components could vary depending on the depth of the tissue section. Therefore, we acknowledge that the clinically relevant contribution of different tumor compartments can only be accurately assessed following the first human tracer injection.

The favorable results from this follow-up study position Nb15-s775z

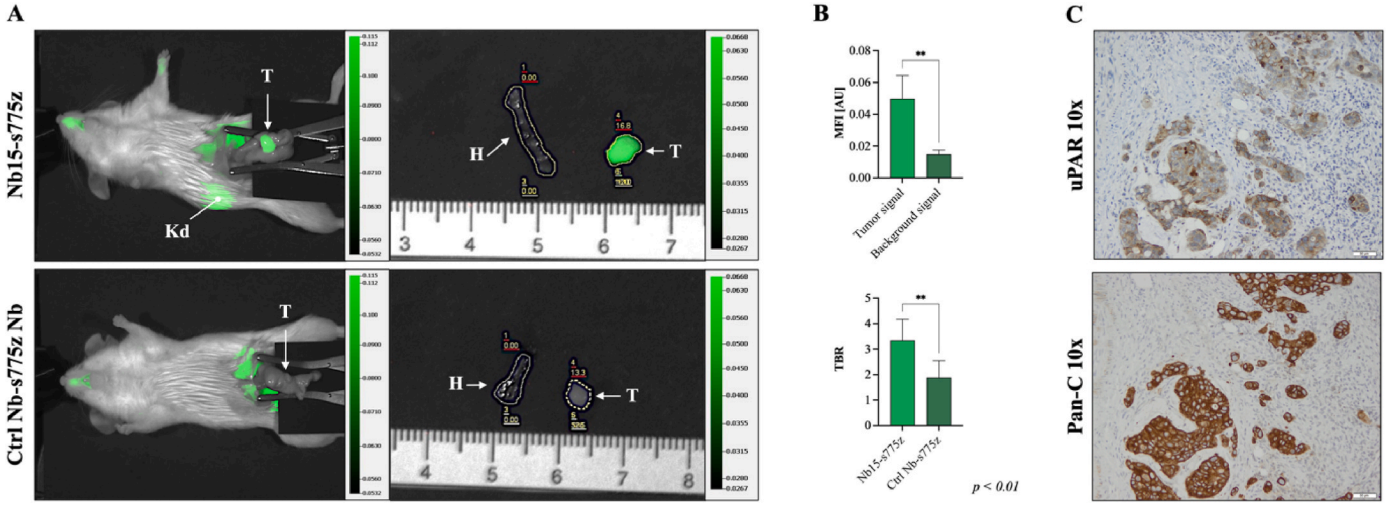

Fig. 3. (A) *In situ* and *ex vivo* NIR imaging to assess the distribution of targeting Nb15-s775z and non-targeting control Nb-s775z in mice bearing CDX colorectal tumors. *T* indicates tumor, *Kd* indicates kidney, and *H* indicates healthy tissue. **(B)** Evaluation of the *ex vivo* signal intensity for the targeting Nb, and comparison of TBRs obtained for the evaluated tracers. Error bars depict SD. **(C)** Microscopic visualization of IHC staining on consecutive tumor slices shows brown staining of tumor cells expressing uPAR (targeted receptor) overlapping with malignant epithelial cells stained by pan-cytokeratin (Pan-C). (For interpretation of the references to color in this figure legend, the reader is referred to the Web version of this article.)

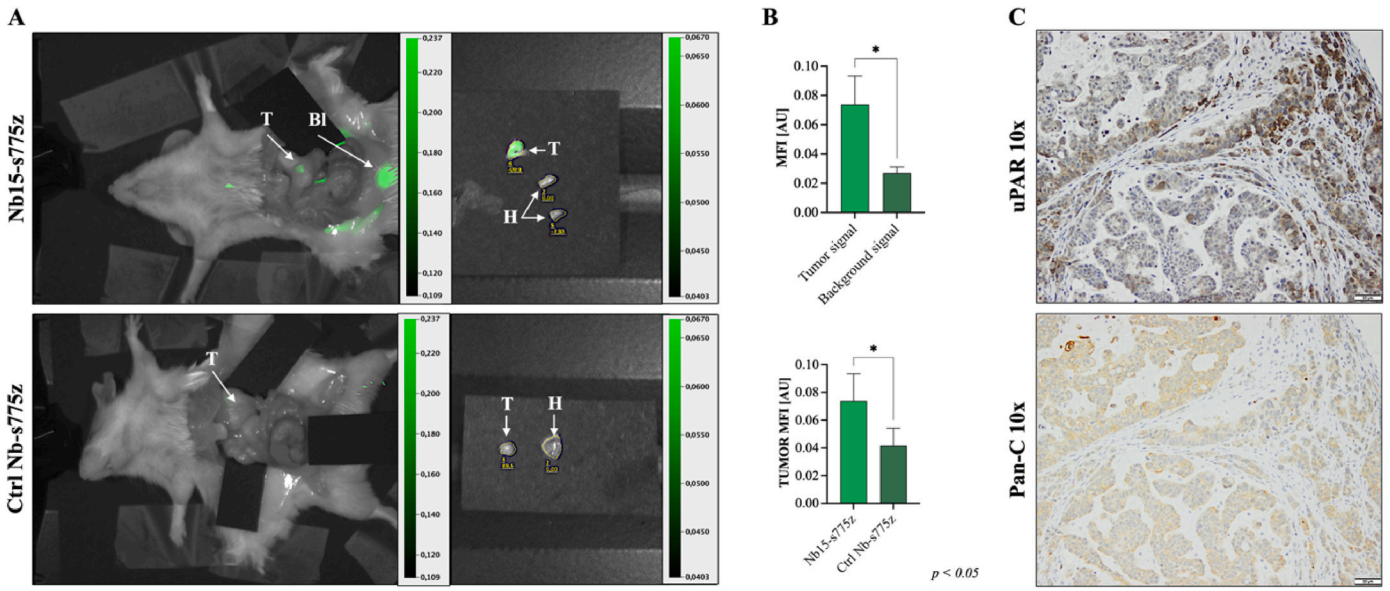

Fig. 4. **(A)** *In situ* and *ex vivo* NIR imaging to assess the distribution of targeting Nb15-s775z and non-targeting control Nb-s775z in mice bearing PDX orthotopic gastric tumors. *T* indicates tumor, *Bl* indicates a urinary bladder, and *H* indicates healthy tissue. **(B)** Evaluation of the *ex vivo* signal intensity for the targeting Nb, and comparison of tumor signals obtained for mice injected with Nb15-s775z or non-targeting control Nb-s775z. Error bars depict SD. **(C)** Microscopic visualization of IHC staining on consecutive tumor slices shows brown staining of tumor cells expressing uPAR (targeted receptor) overlapping with malignant epithelial cells stained ochre against pan-cytokeratin (Pan-C). (For interpretation of the references to color in this figure legend, the reader is referred to the Web version of this article.)

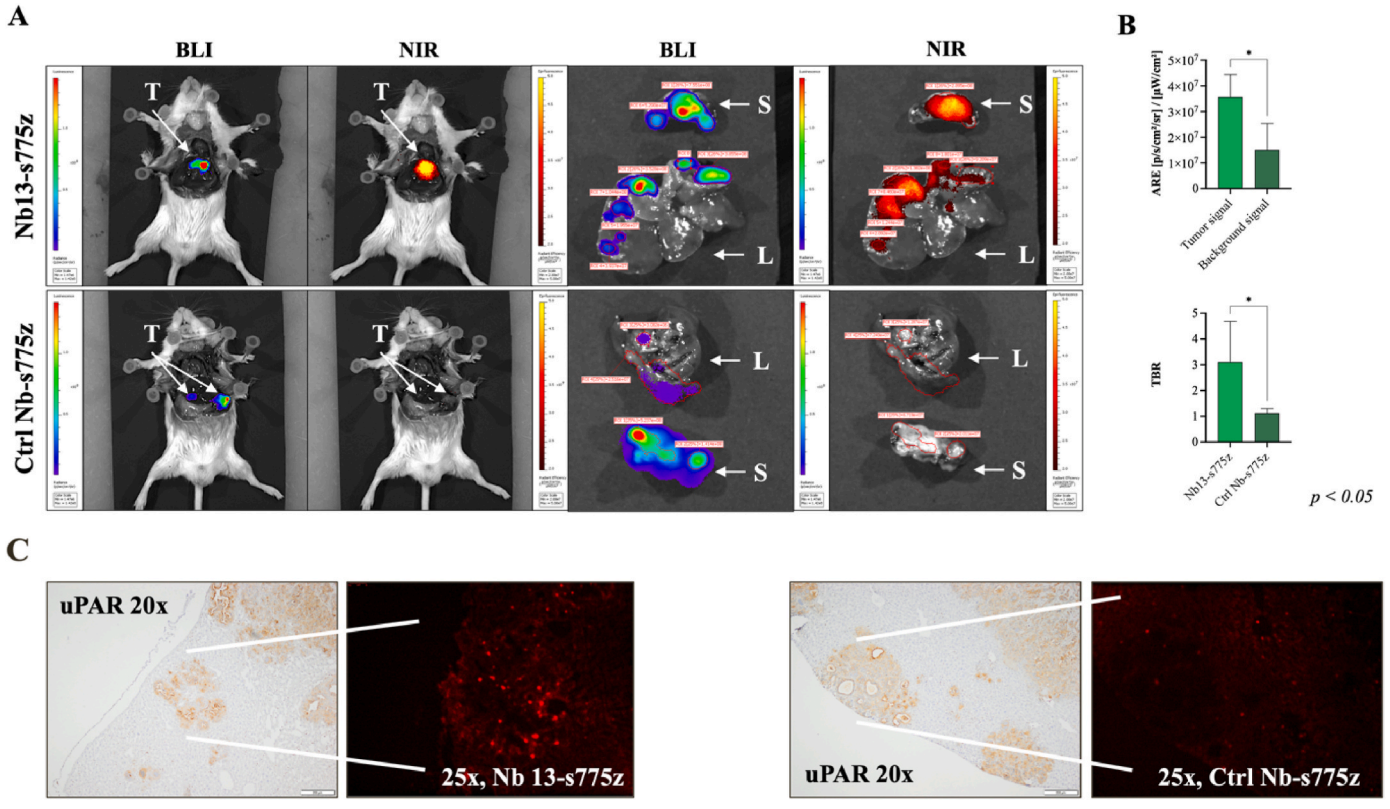

Fig. 5. **(A)** *In situ* (left) and *ex vivo* (right) BLI for monitoring cancer progression and NIR imaging for assessing the distribution of targeting Nb13-s775z and non-targeting control Nb-s775z in mice with CDX splenic tumors and liver metastases. *T* indicates tumor, *S* indicates spleen, and *L* indicates liver. **(B)** Evaluation of the *ex vivo* signal intensity for the targeting Nb, and comparison of TBRs obtained for the tested tracers. Error bars depict SD. **(C)** Microscopic analysis of liver metastases involves targeting and controlling Nbs-s775z. IHC highlights uPAR-positivity in brown, while a red fluorescence signal in the 800 nm channel shows accumulation of the fluorophore. (For interpretation of the references to color in this figure legend, the reader is referred to the Web version of this article.)

on par with the recently developed peptide AE344-IRDye800CW [24], achieving effective tumor illumination within just 1 h post-injection. In contrast, clinically tested fluorescent AE105-ICG (the mother compound of AE344) is injected either 6 h before brain surgery [25] or the day before for oral and oropharyngeal cancer (EudraCT number 2022-001361-12). The fast accumulation is particularly sought-after for FGS, where minimizing the interval between tracer injection and the commencement of surgery is paramount and offers economical advantage. As previously speculated regarding the uPAR expression across diverse cancer types, this study corroborates the broad application potential of anti-uPAR tracers by including CRC, GC, PC and PC-M models. We are confident that the application of the generated Nbs holds promise for extending targeting to various other solid tumors. This potential arises from the receptor's specificity for tissue inflammation and remodeling, which are characteristic for cancer proliferation, rather than cancer cells of specific origin.

We further explored the binding properties of high-affinity anti-HuPAR Nb15 to better understand its *in vivo* behavior. Our objective was to determine the Nb's binding domain and assess any competitive interactions with uPA, the natural uPAR ligand. Flow cytometry revealed that domain D1, prone to protease cleavage, is crucial for Nb binding. Importantly, the domain proven to be indispensable for the positive control (monoclonal antibody generated against D2D3) to retain its high affinity (Fig. 1A). This suggests D1 may be the direct binding site of Nb15 or necessary for maintaining the receptor's molecular organization that enables binding in the most thermodynamically optimal manner. Next, through SPR, we further tested the anti-HuPAR Nb15 for potential competition with the ATF which is the uPA fragment directly responsible for receptor binding [26]. The analysis showed Nb15 has a faster association rate than the ATF ($16.4*10^5$ vs $6.2*10^5$ $M^{-1}s^{-1}$ [15, 22]), indicating more rapid receptor occupancy. Furthermore, Nb15 partially competes with ATF for uPAR binding (Fig. 1B). These results suggest Nb15 could outcompete ATF and requires lower concentrations for effective tumor targeting.

Given that ATF requires residues extending from all three receptor domains for effective binding [9] and competes partially with the tested Nb which loses its binding properties upon D1 cleavage, we speculate that these moieties bind at least partially to approximately the same area (with Nbs requiring amino acids from D1). We acknowledge that interpreting these results to distinguish between steric hindrance and actual binding to the same epitope on HuPAR is challenging. Additional evidence showing hindered binding of the positive control upon D1 cleavage supports the assertion that the presence of D1 is crucial for maintaining the high binding capacity of all uPAR binders. However, to precisely identify the binding sites of the Nb on the receptor, further crystallography studies, similar to those previously performed showing the receptor bound to an antagonist peptide [27], are necessary.

Although the possible disadvantage due to D1 domain shedding, opting for binding domains D2 and D3 is not necessarily a superior alternative with respect to the purpose of tumor imaging. These domains are exclusively responsible for binding to other proteins such as integrins, GPCRs, and tyrosine kinases [28]. Furthermore, the *in vitro* shedding rate corresponds to a complete receptor turnover rate of approximately 24 h [29]. Based on the rapid imaging (observed 1 h post-injection) with the anti-uPAR Nbs previously reported, coupled with the absence of apparent obstacles such as limited tracer uptake or an elevated background signal due to shedding of the tracer-bound domain in this study, we conclude that receptor-level interaction does not hinder fast molecular imaging post-injection.

On the contrary, AE105, currently undergoing clinical translation post-conjugation to radionuclides [30–32] or fluorescent dyes [33], was crafted with the aim of attaining anti-tumor activity through competitive inhibition of uPA binding. A drawback of this approach in terms of molecular imaging, compared to our Nbs, is its inability to displace previously formed uPA-uPAR complexes [34]. However, contrary to theoretical expectations, this *in vivo* behavior did not hinder AE105 from achieving significant *in vivo* binding [35–37], as complete receptor occupation by uPA and full binding prevention is unlikely to happen *in vivo*.

Furthermore, our combination of *in vitro* and *in vivo* data substantiates that partial or full cleavage of this membrane-associated protein does not impede our Nb's ability to target the shed domain specifically. Drawing on our collective experience and previously documented outcomes, we again postulate that uPAR exhibits significant potential for applications in FGS.

5. Conclusion

This study further characterizes the receptor binding of previously generated anti-uPAR Nb15 and validates its fluorescently-labeled versions, which effectively localize primary tumors in CRC, GC, and PC models. Additionally, Nb13 is shown to detect pancreatic cancer metastases in the liver. Our findings show that receptor hindrances do not prevent the Nb15 from accumulating in cancer lesions, enabling rapid FLI within 1 h of tracer injection. The promising performance of these tracers suggests their potential for preclinical and clinical use, particularly for real-time surgical guidance in cancer, including metastatic forms, enhancing tumor resection accuracy and metastasis detection, with potential to improve patient survival.

CRediT authorship contribution statement

Łukasz Mateusiak: Conceptualization, Data curation, Formal analysis, Funding acquisition, Investigation, Methodology, Project administration, Supervision, Visualization, Writing – original draft, Writing – review & editing. **Sarah Hakuno:** Investigation, Methodology. **Eveline S.M. de Jonge-Muller:** Investigation, Methodology. **Sam Floru:** Investigation, Methodology. **Cornelis F.M. Sier:** Conceptualization, Formal analysis, Project administration, Supervision, Writing – review & editing. **Lukas J.A.C. Hawinkels:** Conceptualization, Formal analysis, Funding acquisition, Project administration, Resources, Software, Supervision, Writing – review & editing. **Sophie Hernot:** Conceptualization, Formal analysis, Funding acquisition, Project administration, Resources, Software, Supervision, Writing – original draft, Writing – review & editing.

Ethics approval and consent to participate

All animal experiments were approved by the Dutch central committee on animal experimentation (permit AVD 116002017858 and 16549) and the Animal Welfare Body (IvD) of the LUMC (research protocols 17.038.043, 16549.03.005 and 16549.03.006).

Data availability

The datasets are stored internally according to the data management plan of Vrije Universiteit Brussel and uploaded to PURE – a Current Research Information System (https://researchportal.vub.be). They are available upon request.

Competing interests

With the exception of Mr. Lukasz Mateusiak and Prof. Sophie Hernot, none of the authors have conflicts of interest or financial disclosures. The aforementioned authors specifically acknowledge that they hold a patent for Anti-urokinase plasminogen activator receptor immunoglobulin single variable domains, under EP22199885.9.

Competing interests

I hereby declare, that with the exception of Mr. Lukasz Mateusiak and Prof. Sophie Hernot, none of the authors have conflicts of interest or

financial disclosures. The aforementioned authors specifically acknowledge that they hold a patent for Anti-urokinase plasminogen activator receptor immunoglobulin single variable domains, under EP22199885.9.

Acknowledgements

We thank Leonie G. Plug for her excellent technical support, Andrew Mazar, PhD, Attenuon LLC, San Diego, USA, for providing the anti-HuPAR antibody (clone ATN-617), Massimo Resnati, IRCCS Ospedale San Raffaele, Milan, Italy, for providing the variants of HEK cells, and the Department of Surgery at LUMC for providing the BxPC3 luc2+ cells.

This work was supported by SofinaBoël Fund, Stichting Tegen Kanker (grant number ANI183), Research Foundation – Flanders: Strategic Basic Research program (grant number FWOSBO42), Strategic Research Program (grant number SRP50), Innovation Research Fund (grant number IOF3005), Flanders Agency for Research and Innovation (VLAIO) (HBC.2018.2002), Wetenschappelijk Fonds Willy Gepts (WFWG2023) of the UZ Brussel and Award Cancer Research 2023 - Oncology Center Vrije Universiteit Brussel, funded by the bequests of late Ms. Esther Desmedt and late Ms. Irma Noë.

Appendix A. Supplementary data

Supplementary data to this article can be found online at https://doi.org/10.1016/j.ejso.2024.109537.

References

[1] Mieog JSD, Achterberg FB, Zlitni A, Hutteman M, Burggraaf J, Swijnenburg RJ, et al. Fundamentals and developments in fluorescence-guided cancer surgery. Nat Rev Clin Oncol 2022 Jan 7;19(1):9–22.
[2] FDA approves new imaging drug to help identify ovarian cancer lesions [internet]. Available from: https://www.fda.gov/news-events/press-announcements/fda-approves-new-imaging-drug-help-identify-ovarian-cancer-lesions; 2021.
[3] Tanyi JL, Randall LM, Chambers SK, Butler KA, Winer IS, Langstraat CL, et al. A phase III study of pafolacianine injection (OTL38) for intraoperative imaging of folate receptor-positive ovarian cancer (study 006). J Clin Oncol 2022;41(2):276–84.
[4] Kennedy GT, Azari FS, Bernstein E, Nadeem B, Chang A, Segil A, et al. Targeted detection of cancer cells during biopsy allows real-time diagnosis of pulmonary nodules. Eur J Nucl Med Mol Imag 2022;49(12):4194–204.
[5] CYTALUX® for lung and ovarian cancer surgery [Internet]. [cited 2023 Feb 15]. Available from: https://cytalux.com/.
[6] Rudzińska M, Parodi A, Soond SM, Vinarov AZ, Korolev DO, Morozov AO, et al. The role of cysteine cathepsins in cancer progression and drug resistance. Int J Mol Sci 2019;20(14).
[7] FDA. FDA approves imaging drug to assist in detection of cancerous tissue following lumpectomy. 2024.
[8] Seah D, Cheng Z, Vendrell M. Fluorescent probes for imaging in humans: where are we now? ACS Nano 2023.
[9] Smith HW, Marshall CJ. Regulation of cell signalling by uPAR. Nat Rev Mol Cell Biol 2010 Jan;11(1):23–36.
[10] Mahmood N, Mihalcioiu C, Rabbani SA. Multifaceted role of the urokinase-type plasminogen activator (uPA) and its receptor (uPAR): diagnostic, prognostic, and therapeutic applications. Front Oncol 2018;8(FEB).
[11] Zhai BT, Tian H, Sun J, Zou JB, Zhang XF, Cheng JX, et al. Urokinase-type plasminogen activator receptor (uPAR) as a therapeutic target in cancer. J Transl Med 2022;20(1):1–24. https://doi.org/10.1186/s12967-022-03329-3 [Internet]. Available from:.
[12] Boonstra MC, Prakash J, Van De Velde CJH, Mesker WE, Kuppen PJK, Vahrmeijer AL, et al. Stromal targets for fluorescent-guided oncologic surgery. Front Oncol 2015;5(NOV):1–8.
[13] de Geus SWL, Boogerd LSF, Swijnenburg RJ, Mieog JSD, Tummers WSFJ, Prevoo HAJM, et al. Selecting tumor-specific molecular targets in pancreatic adenocarcinoma: paving the way for image-guided pancreatic surgery. Mol Imag Biol 2016;18(6):807–19.
[14] Christensen A, Grønhøj C, Jensen JS, Lelkaitis G, Kiss K, Juhl K, et al. Expression patterns of uPAR, TF and EGFR and their potential as targets for molecular imaging in oropharyngeal squamous cell carcinoma. Oncol Rep 2022;48(2).
[15] Mateusiak Ł, Floru S, De Groof TWM, Wouters J, Declerck NB, Debie P, et al. Generation and characterization of novel Pan-cancer anti-uPAR fluorescent nanobodies as tools for image-guided surgery. Adv Sci 2024 Jun 6 [Internet]. Available from: https://onlinelibrary.wiley.com/doi/10.1002/advs.202400700.
[16] Muyldermans S. Applications of nanobodies. Annu Rev Anim Biosci 2021 Feb 16;9(1):401–21.
[17] Lemaire M, D'Huyvetter M, Lahoutte T, Van Valckenborgh E, Menu E, De Bruyne E, et al. Imaging and radioimmunotherapy of multiple myeloma with anti-idiotypic Nanobodies. Leukemia 2014;28(2):444–7.
[18] Debie P, Van Quathem J, Hansen I, Bala G, Massa S, Devoogdt N, et al. Effect of dye and conjugation chemistry on the biodistribution profile of near-infrared-labeled nanobodies as tracers for image-guided surgery. Mol Pharm 2017;14(4):1145–53.
[19] Paauwe M, Schoonderwoerd MJA, Helderman RFCP, Harryvan TJ, Groenewoud A, Van Pelt GW, et al. Endoglin expression on cancer-associated fibroblasts regulates invasion and stimulates colorectal cancer metastasis. Clin Cancer Res 2018 Dec 15;24(24):6331–44.
[20] Rabbani SA, Ateeq B, Arakelian A, Valentino ML, Shaw DE, Dauffenbach LM, et al. An anti-urokinase plasminogen activator receptor antibody (ATN-658) blocks prostate cancer invasion, migration, growth, and experimental skeletal metastasis in vitro and in vivo. Neoplasia 2010;12(10):778–88.
[21] Bauer TW, Liu W, Fan F, Camp ER, Yang A, Somcio RJ, et al. Targeting of urokinase plasminogen activator receptor in human pancreatic carcinoma cells inhibits c-Met- and insulin-like growth factor-I receptor-mediated migration and invasion and orthotopic tumor growth in mice. Cancer Res 2005 Sep 1;65(17):7775–81.
[22] Lin L, Gårdsvoll H, Huai Q, Huang M, Ploug M. Structure-based engineering of species selectivity in the interaction between urokinase and its receptor: implication for preclinical cancer therapy. J Biol Chem 2010;285(14):10982–92.
[23] Ahn SB, Chan C, Dent OF, Mohamedali A, Kwun SY, Clarke C, et al. Epithelial and stromal cell urokinase plasminogen activator receptor expression differentially correlates with survival in rectal cancer stages B and C patients. PLoS One 2015 Feb 18;10(2).
[24] Kurbegovic S, Juhl K, Sørensen KK, Leth J, Willemoe GL, Christensen A, et al. IRDye800CW labeled uPAR-targeting peptide for fluorescence-guided glioblastoma surgery: preclinical studies in orthotopic xenografts. Theranostics 2021;11(15):7159–74.
[25] Skjøth-Rasmussen J, Azam A, Larsen CC, Scheie D, Juhl K, Kjaer A. A new uPAR-targeting fluorescent probe for optical guided intracranial surgery in resection of a meningioma—a case report. Acta Neurochir (Wien) [Internet] 2021;164(1):267–71. https://doi.org/10.1007/s00701-021-05051-3. Available from:.
[26] Smith HW, Marshall CJ. Regulation of cell signalling by uPAR. Nat Rev Mol Cell Biol 2010 Jan;11(1):23–36 [Internet]. [cited 2020 Jun 19];Available from: http://www.nature.com/articles/nrm2821.
[27] Llinas P, Hé Lè, Ne Le Du M, Gå Rdsvoll H, Danø K, Ploug M, et al. Crystal structure of the human urokinase plasminogen activator receptor bound to an antagonist peptide. EMBO J 2005;24:1655–63 [Internet]. [cited 2020 Jun 11];Available from: www.embojournal.org.
[28] Mahmood N, Mihalcioiu C, Rabbani SA. Multifaceted role of the urokinase-type plasminogen activator (uPA) and its receptor (uPAR): diagnostic, prognostic, and therapeutic applications. Front Oncol 2018;8(FEB).
[29] Sidenius N, Sier CFM, Blasi F. Shedding and cleavage of the urokinase receptor (uPAR): identification and characterisation of uPAR fragments in vitro and in vivo. FEBS Lett 2000;475(1):52–6.
[30] Carlsen EA, Loft M, Loft A, Berthelsen AK, Langer SW, Knigge U, et al. Prospective phase II trial of prognostication by 68 Ga-NOTA-AE105 uPAR PET in patients with neuroendocrine neoplasms: implications for uPAR-targeted therapy. J Nucl Med 2022;63(9):1371–7.
[31] Fosbøl MØ, Mortensen J, Petersen PM, Loft A, Madsen J, Kjaer A. uPAR PET/CT for prognostication and response assessment in patients with metastatic castration-resistant prostate cancer undergoing radium-223 therapy: a prospective phase II study. Diagnostics 2021;11(6):1087.
[32] Risør LM, Clausen MM, Ujmajuridze Z, Farhadi M, Andersen KF, Loft A, et al. Prognostic value of urokinase-type plasminogen activator receptor PET/CT in head and neck squamous cell carcinomas and comparison with 18F-fdg PET/CT: a single-center prospective study. J Nucl Med 2022;63(8):1169–76.
[33] Skjøth-Rasmussen J, Azam A, Larsen CC, Scheie D, Juhl K, Kjaer A. A new uPAR-targeting fluorescent probe for optical guided intracranial surgery in resection of a meningioma—a case report. Acta Neurochir 2021;164(1):267–71.
[34] Baart VM, Boonstra MC, Sier CFM. uPAR directed-imaging of head-and-neck cancer News. Oncotarget 2017;8(9):20519–20.
[35] Albrechtsen M. FluoGuide announces FG001 meets primary endpoint in phase llb trial in aggressive brain cancer.
[36] Albrechtsen M. FluoGuide receives FDA orphan drug designation for FG001 in high-grade glioma [Internet]. Available from: https://fluoguide.com/mfn_news/fluoguide-receives-fda-orphan-drug-designation-for-fg001-in-high-grade-glioma/; 2023.
[37] Albrechtsen M. FluoGuide confirms positive topline results from phase lla trial of FG001 in head & neck cancer at International Academy of Oral Oncology conference [Internet]. Available from: https://fluoguide.com/mfn_news/fluoguide-confirms-positive-topline-results-from-phase-lla-trial-of-fg001-in-head-neck-cancer-at-international-academy-of-oral-oncology-conference/.

Further reading

[1] Schoonderwoerd MJA, Hakuno SK, Sassen M, Kuhlemaijer EB, Paauwe M, Slingerland M, et al. Targeting endoglin expressing cells in the tumor microenvironment does not inhibit tumor growth in a pancreatic cancer mouse model. OncoTargets Ther 2021;14:5205–20.